Ocean Engineering 334 (2025) 121619

Contents lists available at ScienceDirect

Ocean Engineering

journal homepage: www.elsevier.com/locate/oceaneng

Research paper

A neural network framework for extrapolating sea surface spectra from wave pressure signals

Nikolas Martzikos, Giovanni Malara, Felice Arena *

Natural Ocean Engineering Laboratory (NOEL), "Mediterranea'' University of Reggio Calabria, Loc. Feo di Vito, 89122, Reggio Calabria, Italy

ARTICLE INFO

Keywords:
Artificial neural networks
Machine learning
Sea surface elevation
Pressure

ABSTRACT

This study investigates the prediction of sea surface elevation spectra from pressure measurements using frequency-specific artificial neural networks (ANNs). Unlike traditional time-domain approaches, the proposed methodology employs spectral analysis to decompose pressure signals into discrete frequency components and applies compressive sampling for outlier handling at the preprocessing stage. A separate ANN is trained for each frequency, utilising the water depth and other scalar features—including the statistical properties of the pressure head (mean, variance, peak period, and the narrow-bandedness parameter) - as inputs. The models are trained on 3005 samples, validated on 1252 samples, and tested on 751 samples. After model development, the ANNs were applied to a separate set of 100 previously unseen samples to evaluate the extrapolation framework. Model performance was assessed using a comprehensive set of error metrics. Results indicate that incorporating spectral features of pressure signals into ANN architectures provides a robust and efficient framework for sea surface spectra prediction, with potential applications in ocean and coastal engineering.

1. Introduction

Understanding and predicting hydrodynamic processes are essential for the design and operation of coastal and offshore infrastructure in ocean engineering. These applications include wave energy converters, offshore wind farms, maritime transport, and port structures that operate in dynamic marine environments. Ensuring their safety, efficiency, and durability requires detailed investigations of wave-structure interactions, hydrodynamic and mooring loads, and free surface dynamics. Both physical and numerical experiments are widely used for this purpose. Experimental data are fundamental for model validation and refinement. Physical experiments generally provide higher accuracy but require greater resources and are therefore preferred when available. However, data collection in ocean engineering experiments is often affected by sensor failures, environmental conditions, and data transmission errors. Missing or incomplete measurements create challenges in wave analysis, where gaps or inaccuracies in signals affect the accuracy of estimated variables. Traditional approaches, including autoregressive moving average (ARMA) models (Box et al., 2015), which have been widely applied in fields such as oceanography (Ge and Kerrigan, 2016; Martzikos and Soukissian, 2017), statistical methods such as Kalman filtering (Evensen, 2003) and interpolation (Gambarelli et al., 2024), and analytical techniques based on deterministic formulations, such as Fourier analysis (Laface et al., 2017; Massel, 2001) and differential equations (Strogatz, 2014), have been used to refine and reconstruct time series data by leveraging temporal dependencies. In contrast, compressive sampling (CS), a sparsity-driven framework, offers an alternative approach for recovering signals from incomplete data (Candes and Wakin, 2008; Donoho, 2006; Malara, 2022). These methods provide useful approximations and can also be employed for short-term forecasting. However, they are constrained by fixed mathematical assumptions, which may limit their effectiveness in capturing complex physical processes.

To address these limitations, data-driven approaches, enhanced by advancements in artificial intelligence (AI), have gained attention for their ability to model complex nonlinear relationships efficiently in ocean engineering (Panda, 2023; Portillo Juan et al., 2023; Portillo Juan and Negro Valdecantos, 2022). AI techniques, particularly artificial neural networks (ANNs), have enabled significant progress in applications such as forecasting (Fan et al., 2020; Jörges et al., 2021; Kagemoto, 2020), load dynamics (Li and Choung, 2017; Martzikos et al., 2024; Sidarta et al., 2019), and signal reconstruction (Durán-Rosal et al., 2016; Li et al., 2025). Other methods, including deep neural networks (DNNs), long short-term memory models (LSTM), convolutional neural networks

* Corresponding author.
E-mail addresses: nikolas.martzikos@unirc.it (N. Martzikos), giovanni.malara@unirc.it (G. Malara), *arena@unirc.it* (F. Arena).

https://doi.org/10.1016/j.oceaneng.2025.121619
Received 2 April 2025; Received in revised form 12 May 2025; Accepted 19 May 2025
0029-8018/© 2025 The Authors. Published by Elsevier Ltd. This is an open access article under the CC BY license (http://creativecommons.org/licenses/by/4.0/).

(CNNs), genetic algorithm-assisted CNNs (GA + CNN), and random forests, have also demonstrated effectiveness in similar domains (Campos et al., 2021; Minuzzi and Farina, 2024; Wei and Davison, 2022; Yuan et al., 2024; Zanganeh, 2017). By leveraging large datasets, these approaches provide flexible and adaptive solutions that can outperform traditional analytical models.

One specific application of AI in ocean engineering is predicting sea surface elevation (SSE) from pressure head records, especially when missing data disrupt the signal or when outliers introduce inconsistencies that need correction. Traditional methods, such as CS, are widely used for wave signal reconstruction by relying on signal sparsity and are limited to filling gaps or extrapolating data via a predetermined representation of the process under examination (Malara, 2022; Malara et al., 2018). In contrast, ANNs provide a data-driven alternative that adapts to nonlinear and nonstationary relationships, making them more efficient in reconstructing the entire time series if required. Additionally, they can handle scattered missing data points rather than just sequential gaps, as often caused by sensor failures.

This study develops a framework that utilises spectral features of pressure signals to predict SSE, providing a data-driven alternative to time-domain and analytical methods. By decomposing pressure signals into discrete frequency components, the proposed approach enables a more detailed representation of wave characteristics. The findings have important implications for oceanographic modelling and the reliability of experimental observations in marine environments. In particular, this study serves as a basis for the construction of low-cost monitoring systems to be employed in coastal areas or in the vicinity of marine infrastructures. In this context, typical tools utilised for monitoring purposes are wave buoys, acoustic doppler current profilers (ADCP), satellite observations, high-frequency (HF) coastal radars, and shipboard observations, that are adopted with the purpose of estimating relevant statistical quantities, such as significant wave height and mean wave periods and directions (Pandian et al., 2010). Also, other notable options are available, such as the stereo – cameras (Benetazzo et al., 2012). However, they are generally characterised by high costs of the equipment and, in case of stereo-cameras, by the need of highly performant post-processing units. Instead, sensors measuring water pressures are widely accessible even for low budget projects and do not have exorbitant computational requirements. Thus, they are ideal tools for building a low-cost wave measurement station.

The objective of this study is to assess the reliability of ANNs for predicting SSE from pressure head signals in the frequency domain. To this end, a modular frequency-domain neural network framework is proposed. Unlike previous approaches that typically operate in the time domain or rely on a single global model, the proposed method trains a distinct ANN for each spectral component. This architecture, based on the analytical independence of wave frequencies, allows each ANN to be independently trained, validated, and tuned. This modular approach facilitates systematic performance assessment across the spectrum, making it easier to detect underperforming models or anomalies and thus contributing to a more reliable framework. The use of field-measured pressure spectra as input increases the relevance of the framework for practical ocean monitoring applications, in contrast to methods relying on synthetic datasets. To the authors' knowledge, this represents a novel application of ANNs for full-spectrum SSE extrapolation in the frequency domain from pressure data, based on an ensemble of frequency-specific models.

The remainder of this paper is structured as follows. Section 2 details the methodology, including theoretical background, data collection, data processing and feature extraction, model development, and the evaluation of the extrapolation framework. Section 3 presents the results and discussion, analysing overall performance using key error metrics. Finally, Section 4 summarises the main findings, discusses potential applications, and outlines future research directions.

2. Methodology

The methodological framework combines theoretical foundations and machine learning techniques. As a first step, the classical approach to deriving wave elevation spectra from pressure spectra is outlined, and its limitations—particularly its sensitivity to high-frequency attenuation—are discussed, motivating the development of the ANN-based method presented here. The development and evaluation of the proposed ANNs follow a structured process: beginning with data collection in the time domain, followed by preprocessing and feature extraction involving outlier correction, frequency-domain transformation, and feature normalisation. The data are then divided into frequency components and used to train ANNs corresponding to each frequency. The overall performance of the extrapolation framework is subsequently evaluated using a separate set of 100 previously unseen records.

2.1. Theoretical background and limitations

Random water wave fields are commonly represented via spectral representation under the assumption that the wave field is a Gaussian stationary ergodic random process (Ochi, 1998). Therefore, sea surface displacement $\eta(t)$ and wave pressure heads $p_h(z,t)$, at a given water depth z, can be expressed as the superposition of a large number N of harmonic components, as follows:

$$\eta(t) = \sum_{i=1}^{N} a_i \cos(\omega_i t + \varepsilon_i), \tag{1}$$

and

$$p_h(z,t) = \sum_{i=1}^{N} a_i \frac{\cosh[k_i(d+z)]}{\cosh(k_i d)} \cos(\omega_i t + \varepsilon_i), \tag{2}$$

where a_i denotes the amplitude, ω_i the radian wave frequencies all different from each other, ε_i a random phase angle uniformly distributed in $[0, 2\pi)$, d is the total water depth, and k_i is the wave number associated with the wave frequency through the linear dispersion rule:

$$k_i \tanh(k_i d) = \frac{\omega_i^2}{g}, for\ i = 1, \ldots, N \tag{3}$$

where the amplitudes a_i are all infinitesimals of the same order, related to the wave frequencies via the power spectral density function of the free surface displacement process $S_\eta(\omega)$, as expressed by the equation:

$$S_\eta(\omega)\delta\omega = \frac{1}{2}\sum_i a_i^2, for\ \omega - \frac{\delta\omega}{2} < \omega_i < \omega + \frac{\delta\omega}{2} \tag{4}$$

The ratio of hyperbolic cosines in Eq. (2) is commonly called attenuation factor. It is a decaying function of the water depth and renders the physical evidence that the wave pressure head amplitude decays by moving away from the mean water level towards the seabed.

Clearly, sea surface displacement and pressure head can be analysed in frequency domain by Fourier transform of Eq. (1) and of Eq. (2). By doing that, it is seen straightforwardly that the spectra of these quantities are related to each other by the equation:

$$S_{p_h}(\omega) = S_\eta(\omega) \frac{\cosh^2[k(d+z)]}{\cosh^2(kd)}, \tag{5}$$

where $S_{p_h}(\omega)$ denotes the power spectral density function of the wave pressure head p_h.

The direct relationship between $S_\eta(\omega)$ and $S_{p_h}(\omega)$ suggests the idea that only one quantity is sufficient to determine the spectrum of either $\eta(t)$ or $p_h(z,t)$, given that the square of the attenuation factor can be computed directly over the relevant frequency domain. This fact can be used to show a classical result of the sea states theory: the spectra of the wave pressure heads are narrower than the ones of the free surface

displacement. Indeed, the squared attenuation factor in Eq. (5) decays rapidly in the high frequency tail of the spectrum $S_\eta(\omega)$. Thus, rendering the cut-off of the high frequency tail of the wave pressure head spectrum (Boccotti, 2000a). However, the computation of the sea surface displacement spectrum $S_\eta(\omega)$ from a wave pressure head spectrum $S_{p_h}(\omega)$ can be a daunting task. Indeed, the inverse of the attenuation factor is exponentially dependent on the wave frequency ω, so that a direct application of Eq. (5) would lead to a physically inconsistent spectrum in the high frequency region. The methodology described in the following sections allows for circumventing this problem by leveraging a specifically designed ANN architecture.

2.2. Data collection

The dataset utilised in this study was derived from field experiments previously conducted at the Natural Ocean Engineering Laboratory (NOEL) at the Mediterranea University of Reggio Calabria, Italy. NOEL's infrastructure, designed for real-time monitoring of natural sea conditions, facilitated the collection of data under uncontrolled field conditions. These experiments focused on small, wind-driven sea states, characterised by typical significant wave heights ranging from 0.20 m to 0.80 m and peak wave periods between 2.0 and 3.6 s, resembling JONSWAP spectra. The data were extracted from a database comprising records recorded continuously between 2016 and 2018. Specifically, in this work, a sample of collected data between July 15, 2016 and January 3, 2018 was used. Each record is 10 min long with a sampling frequency of 10 Hz, and the measurements were conducted in shallow water, with a total depth of approximately 4 m. The monitoring activity relied on the use of ultrasonic probes placed above the mean water level and on pressure transducers placed below the mean water level under the ultrasonic probe (see Fig. 1). Two ultrasound – pressure transducer pairs have been used during the whole monitoring activity in order to ensure redundancy of measurements. In both cases, the transducer has been placed at a distance of 1.05 m from the seabed, and the ultrasound has been placed at a distance of 2.62 m from the pressure transducer. The two pairs of sensors operated at a distance of 1.44 m, which ensured the absence of mutual interferences between the sensors.

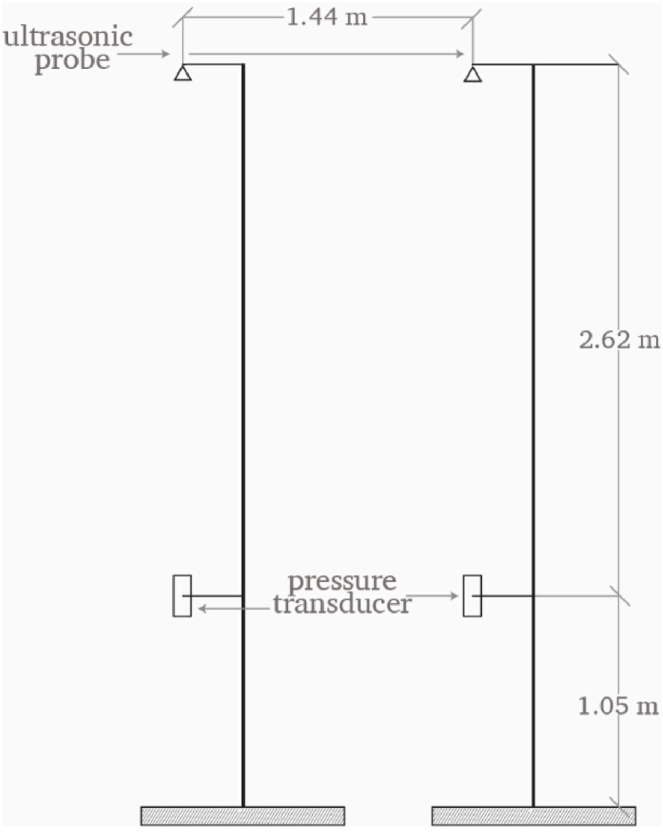

Fig. 1. Sensors used for recording the water pressure (pressure transducers) and the free surface displacement (ultrasonic probes). The pressure transducers were located 1.05 m above the seabed and the ultrasonic probes 2.62 m above the transducers. The total water depth during the measurements was approximately 4 m.

2.3. Data processing and feature extraction

Before processing the data, the signals were checked for outliers that may have been caused by sensor-related discontinuities and anomalies not corresponding to real measurements. To identify these outliers, a conservative threshold was applied based on prior laboratory experience. In this approach, values exceeding the *mean* $\pm$ 5·std were considered outliers and treated as missing data. These were subsequently reconstructed using the CS method described by Candès et al. (2006). This methodology was employed to restore corrupted signals by treating the identified outliers as gaps, thereby enforcing the data reconstruction via an L1-norm minimisation procedure.

Subsequently, the time-domain signals $p_h(z,t)$, $\eta(t)$, representing wave pressure head and sea surface displacement respectively, each consisting of 6000 values per record, were transformed into the frequency domain using the method described by Boccotti et al. (2011). The resulting power spectral density functions, denoted as $S_{p_h}(\omega)$ and $S_\eta(\omega)$, were obtained by applying the Fourier transform of the detrended time series. Prior to transformation, the mean was removed from each signal to eliminate the direct current (DC) component and focus the spectral analysis on dynamic fluctuations. The spectral density was computed by estimating the squared amplitude of the Fourier coefficients, followed by frequency binning to obtain the power spectral density. Both spectra were normalised with respect to the pressure variance and interpolated over a fixed non-dimensional frequency grid comprising 100 values to ensure consistency across records and construed by normalising the dimensional frequency values by the pressure peak frequency value ω_p. Further, following Boccotti et al. (2011), a low-frequency cut-off and a high-frequency cut-off were introduced, respectively, at $0.5\omega_p$ and $5.0\omega_p$. The first frequency allowed excluding from the computation low frequency phenomena, such as tidal variations, that are not relevant in the definition of wind-wave spectra characteristics; the second frequency allowed ignoring the contribution of negligible high frequency components. In this regard, note that typical wind-wave generated seas have a power law decaying pattern ensuring that a negligible energy content is comprised in the frequency band $\omega > 3.0\omega_p$. Therefore, the threshold utilized in this analysis ensures capturing most of the sea frequency content.

In addition to the normalised frequency spectra of the wave pressure and sea surface displacement obtained above, other scalar parameters were computed from both the time and frequency domain to support processing and analysis. These include the peak spectral period T_p, the variance and mean of the measured pressure head signal $p_h(z,t)$, the water depth (d), and the narrow-bandedness parameter ψ^*, providing a comprehensive description of the wave field. The parameter ψ^* is defined as:

$$\psi^* = \left|\frac{\psi(T^*)}{\psi(0)}\right| \tag{6}$$

where ψ is the autocovariance function of the surface elevation time series, T^* is the time lag corresponding to the absolute minimum of function ψ and $\psi(0)$ is the autocovariance at zero lag, which corresponds to the variance of the signal. Lower values of ψ^* indicate broader spectra, while higher values suggest narrower spectral distributions. Based on extensive field measurements at NOEL, Boccotti (2000b)

reported that typical wind-generated waves exhibit ψ^* values within the range of 0.65–0.75, with a value of approximately 0.73 for the mean JONSWAP spectrum. This range is used as a reference when analysing wave conditions, and ψ^* can therefore serve as a reliable indicator for distinguishing purely wind-driven waves from mixed or swell-influenced sea states. This limitation is also considered in the present study to assess the spectral characteristics, resulting in the selection of 5009 files used in this application.

Prior to model development, the aforementioned parameters that were neither already normalised nor inherently confined to the [0,1] range were normalised to ensure consistent scaling across the dataset and uniform magnitude among features. A min-max scaling approach was applied, using the global minimum and maximum values calculated from the entire dataset. Each parameter was transformed according to the formula:

$$x_{norm} = \frac{x - x_{min}}{x_{max} - x_{min}} \tag{7}$$

2.4. Model development

After splitting each record into 100 frequency components, corresponding to specific indices derived from the spectral analysis described in the previous section, a separate dataset was created for each frequency, and an individual ANN was trained for each component, resulting in 100 models. While the framework involves 100 frequency-specific ANNs, these models are not developed in parallel but independently and sequentially, making it easier to detect and isolate performance issues at specific frequencies and reducing the risk of local errors affecting the full-spectrum extrapolation.

An overview of this workflow is illustrated in Fig. 2. The six scalar features used as inputs to the ANN models include: water depth, the value of the power spectral density function of the wave pressure head at each frequency, peak spectral period T_p, variance and mean of the pressure head, and the narrow-bandedness parameter ψ^*.

Accordingly, each of the 100 frequency-specific ANNs is structured with six input nodes (one per feature) and a single output node corresponding to the predicted value of the SSE spectrum $S_\eta(\omega)$ at that frequency. The models were developed and trained in Python using TensorFlow (2024), based on the previously extracted and normalised variables, as summarised in Table 1. The dataset was randomly split to ensure robust training and evaluation, with 60 % (3005 samples) used for training, 25 % (1252 samples) for validation, and 15 % (751 samples) for testing.

Alternative modelling approaches, such as using a single ANN to predict the entire SSE spectrum directly from the pressure spectrum, were initially explored. However, these attempts led to unstable results and limited accuracy. This motivated a different strategy in which each frequency is modelled separately using its own ANN, taking into account the physical interpretation of the wave spectrum. This approach is consistent with conventional practices in ocean engineering, where the frequency components are commonly analysed independently. The resulting architecture improved training stability enabled clearer interpretation of results, and aligned more closely with established wave analysis methods.

Hyperparameter tuning for each model was conducted using Bayesian Optimisation, enabling systematic exploration of the model architecture and training parameters. To identify the most suitable network architecture, 30 Bayesian Optimisation trials were conducted for each frequency model, testing various combinations of nodes, layers, and dropout rates, with the architecture that minimised the validation loss being selected. The tuned hyperparameters and training settings are summarised in Table 2. Key parameters included the number of hidden layers, units per layer, activation functions, dropout rates, and the learning rate, which followed an Exponential Decay schedule to improve convergence.

Table 1
Input features and target variable used for training the frequency-specific ANN models.

Variable	Symbol	Unit	Type
Water depth	d	m	Input
Power spectral density of wave pressure head	$S_{p_h}(\omega)$	m^2/Hz	Input
Wave peak period	T_p	s	Input
Variance of Pressure head	$\sigma^2_{p_h}$	m^2	Input
Mean of Pressure head	μ_{p_h}	m	Input
Narrow-bandedness parameter	ψ^*	–	Input
Power spectral density of sea surface elevation	$S_\eta(\omega)$	m^2/Hz	Target

Table 2
Overview of hyperparameters and training configurations for the ANN models.

Parameter	Value
Batch size	32
Number of epochs	1000
Early stopping patience	10 epochs
Initial learning rate	10^{-4}-10^{-2}
Decay rate of learning rate	0.9
Decay steps	1000
Number of hidden layers	1–3
Units per hidden layer	32–128
Activation functions	ReLU, Tanh, SELU
Dropout rate	0.1–0.3

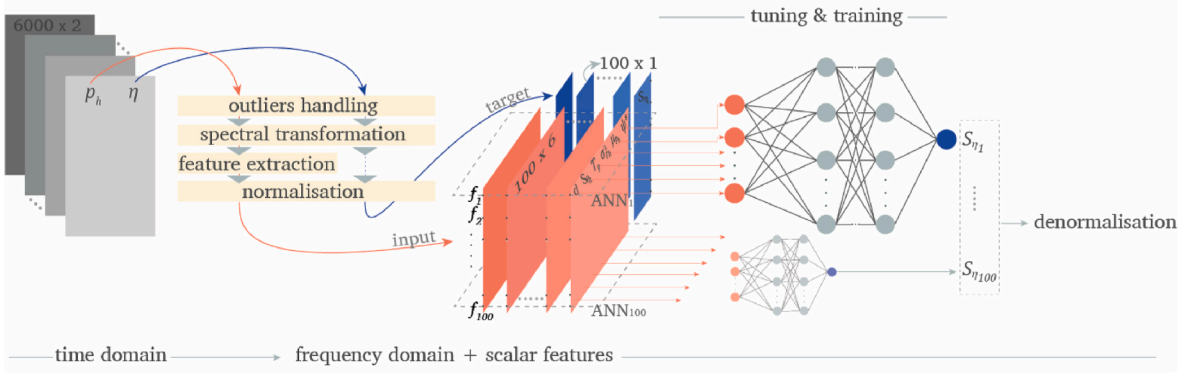

Fig. 2. Workflow for predicting the sea surface elevation spectrum $S_\eta(\omega)$ using frequency-specific ANNs. Each ANN is trained with six scalar input features derived from frequency- and time-domain processing of the wave pressure signal $p_h(z,t)$, including: the pressure spectral density $S_{p_h}(\omega)$, the peak spectral period T_p, the mean and variance of p_h, the water depth d, and the narrow-bandedness parameter ψ^*.

The models were trained using the Adam optimiser with a loss function designed to minimise the squared differences between predicted and actual values. Each network was trained for up to 1000 epochs, with early stopping applied to prevent overfitting. At this phase, cross-validation was not performed, as training 100 ANNs—each corresponding to a specific frequency—already provides insight into model performance variability. The need for cross-validation will be reconsidered if required for a more robust uncertainty estimation.

Model performance was primarily assessed using the Root Mean Square Error (RMSE) and the Normalised Root Mean Square Error (NRMSE), which evaluated the accuracy between predicted and actual values. These metrics are defined as follows:

$$RMSE = \sqrt{\frac{1}{n}\sum_{t=1}^{n}\left(y_{t,predicted} - y_{t,actual}\right)^2} \tag{8}$$

$$NRMSE = \frac{RMSE}{y_{max} - y_{min}} \cdot 100 \tag{9}$$

During training, the Mean Squared Error (MSE) was employed as the loss function to minimize the difference between predicted and actual values. It is defined as:

$$MSE = \frac{1}{n}\sum_{t=1}^{n}\left(y_{t,predicted} - y_{t,actual}\right)^2 \tag{10}$$

Where $y_{t,predicted}$ and $y_{t,actual}$ denote the predicted and actual values of the sea surface elevation spectrum $S_\eta(\omega)$ at the t-th frequency component. The terms y_{max} and y_{min} refer to the global maximum and minimum values of the target spectrum $S_\eta(\omega)$, calculated across all records for each frequency and n is the number of frequency components in the spectrum (i.e., $n = 100$).

2.5. Evaluation of the extrapolation framework

After model development, the trained ANNs were evaluated not only to assess individual model performance, but also to validate the overall extrapolation framework, in which outputs from all 100 frequency-specific models are combined to reconstruct the SSE spectrum. For this purpose, a separate set of 100 previously unseen records was used. These records were randomly selected from the original dataset and were not included in the training, validation, and testing phases. For each record, the input features corresponding to each frequency were fed into the respective ANN, and the resulting predictions were aggregated to reconstruct the complete normalised spectrum.

Following prediction, the outputs were denormalised to restore the original scale of the SSE spectrum. The 100 reconstructed spectra were then compared to the original spectra to evaluate prediction accuracy. This evaluation included the computation of RMSE, NRMSE to quantify differences between the predicted and actual values. In addition, Mean Absolute Error (MAE) was also estimated based on absolute differences:

$$MAE = \frac{1}{n}\sum_{t=1}^{n}\left|y_{t,predicted} - y_{t,actual}\right| \tag{11}$$

To complement the error metrics, the coefficient of determination R^2 was also computed to quantify how well the predicted spectra align with the actual spectra, as follows:

$$R^2 = 1 - \frac{\sum_{t=1}^{n}\left(y_{t,predicted} - y_{t,actual}\right)^2}{\sum_{t=1}^{n}\left(y_{t,actual} - \overline{y}_{actual}\right)^2} \tag{12}$$

Where $y_{t,actual}$, $y_{t,predicted}$ represent the actual and the predicted values of the SSE spectrum $S_\eta(\omega)$ at the t-th frequency component, with $t = 1,\ldots,100$, and $\overline{y}_{actual}$ denotes the mean of the actual spectrum $S_\eta(\omega)$ across frequencies per record.

To complement the numerical results, plots comparing actual and predicted SSE spectra were generated, providing visual insight into the prediction quality across the frequency domain.

3. Results and discussion

The time-domain pressure head $p_h(z,t)$ and sea surface elevation $\eta(t)$ signals, each comprising 6000 samples per record, constitute the dataset used for developing the ANN models. Both signals were first processed to identify and reconstruct anomalies and then transformed into the frequency domain as described in Section 2.3. This transformation resulted in the wave pressure spectrum $S_{p_h}(\omega)$ and the SSE spectrum $S_\eta(\omega)$.

Fig. 3 presents a representative example of these two initial steps (outliers handling and spectral transformation) applied to the $\eta(t)$ signals, where anomaly correction was more frequently required due to the nature of the data. The visual representation of $p_h(z,t)$ signal is omitted here, as they exhibited fewer anomalies and would not offer additional insight. The raw SSE signal (Fig. 3a) shows visible anomalies, which were addressed using the outlier detection and reconstruction method. The corrected signal (Fig. 3b) displays improved continuity, enabling more accurate spectral analysis. Subsequently, the signal was transformed into the frequency domain (Fig. 3c), highlighting the dominant wave components.

After these steps, the normalised $S_\eta(\omega)$ was used as the target variable, and the corresponding pressure head spectrum $S_{p_h}(\omega)$, along with other five extracted scalar features $\left(d, T_p, \sigma^2_{p_h}, \mu_{p_h}, \psi^*\right)$ served as the input to each frequency-specific ANN.

The RMSE during the training process was analysed to characterise the convergence behaviour and performance of the models. The training of the 100 ANNs was optimised using Bayesian optimisation with early stopping to ensure efficient convergence and prevent overfitting. Each model corresponds to a specific frequency component of the SSE spectrum, with the complete frequency-domain representation reconstructed by aggregating the predictions from all 100 models.

Fig. 4 illustrates the number of epochs required for convergence across all frequency models. Most models converged within 20–50 epochs, indicating a stable and efficient training process. A few outliers required over 80 epochs to converge, potentially due to the increased complexity or variability of certain frequency components. Nonetheless, the loss curves for these models (Fig. 5a–c) demonstrated stable convergence, suggesting that the extended training was necessary to capture more subtle spectral features rather than resulting from training instability.

Fig. 6 (a)and (b) show the RMSE and NRMSE values across frequencies. As expected, RMSE values Fig. 6 (a) are higher at lower frequencies due to the larger magnitudes of the target spectrum in this range. However, because RMSE is scale-dependent, it does not allow for direct comparison of model performance across frequencies. Instead, NRMSE provides a normalised measure that enables such comparisons. Fig. 6 (b) shows that NRMSE remains consistently low across most frequencies, with the majority of values below 13 %, and only a few higher outliers at higher frequencies. These results indicate that the training approach and selected hyperparameters were appropriate, supporting the effectiveness of the ANN models for frequency-domain SSE prediction. Moreover, the variation in RMSE across the 100 frequency-specific ANNs is small, as shown in Fig. 6 (a), indicating that the models achieve similar levels of accuracy. This consistency in performance suggests that the training and validation procedure used for each model is sufficient, making additional cross-validation unnecessary for robust uncertainty estimation in this study.

After developing the ANNs, a separate batch of 100 previously unseen records was set aside to evaluate the extrapolation framework, as described in Section 2.5. For each record, the input features corresponding to all frequencies were processed through their respective

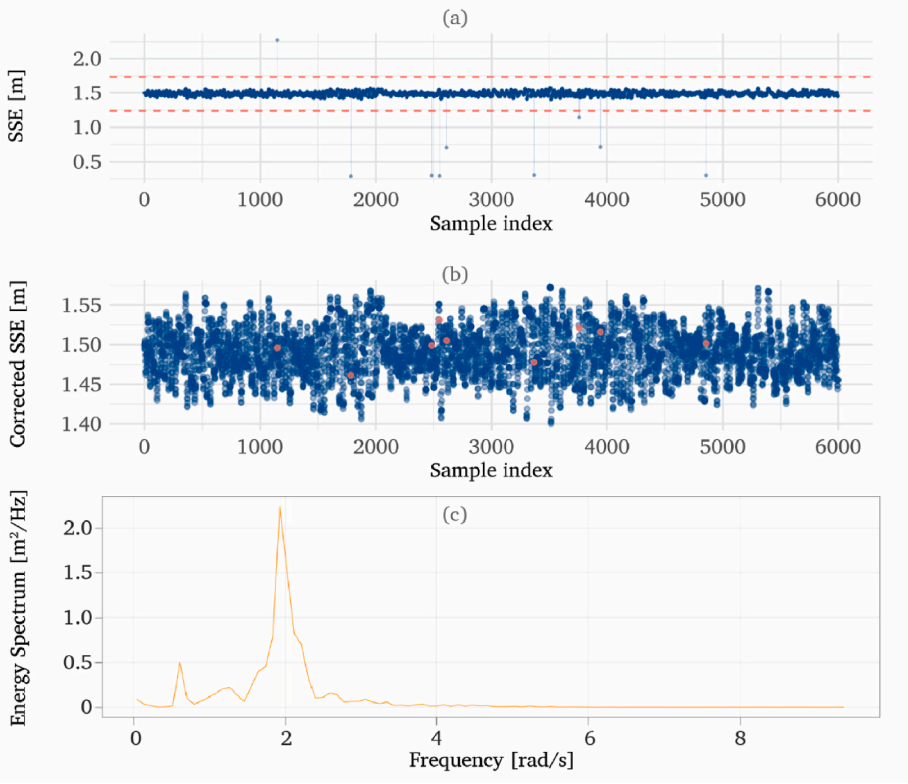

Fig. 3. Sea surface elevation (SSE) signal processing steps: (a) the raw SSE as recorded by the ultrasonic probe in the time domain, (b) the corrected SSE after outlier removal, and (c) the corresponding energy spectrum $S_\eta(\omega)$ obtained through the conversion to the frequency domain.

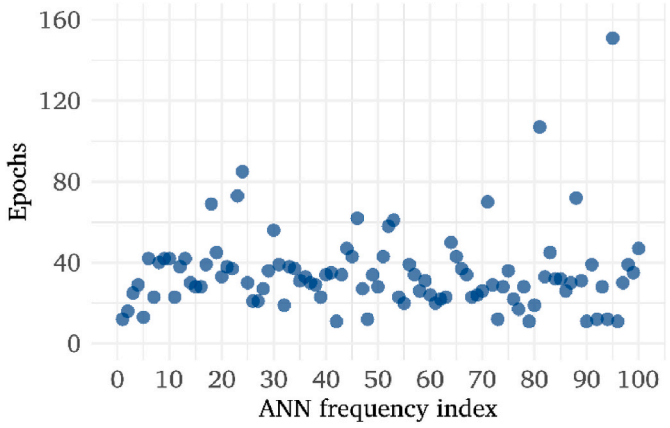

Fig. 4. Number of epochs required to train the ANNs across different frequency indices.

frequency-specific ANNs to predict the SSE spectrum component. These predicted components were then aggregated to reconstruct the full SSE spectrum for each record. To ensure a balanced assessment of prediction accuracy, three error metrics were computed (RMSE, NRMSE, and MAE) by comparing the actual and reconstructed spectra.

Fig. 7 Shows the distribution of these errors across the 100 evaluation records, with a colour gradient representing the narrow-bandedness parameter (ψ^*), to explore whether prediction accuracy is influenced by spectral shape. RMSE and MAE differ in their sensitivity to large errors, as RMSE penalises large deviations more heavily, whereas MAE provides a more direct measure of average absolute error. In this case, this difference affects only the magnitude of the errors, as both metrics exhibit similar distributions in Fig. 7 (a) and 7 (c), with most errors close to zero. Fig. 7 (b) shows that the majority of NRMSE values are below 25 %, although a few cases exceed this threshold, reflecting reduced prediction accuracy in those cases. However, the colour gradient does not reveal a consistent relationship between high error magnitude and ψ^*, suggesting that the narrow-bandedness parameter is not a dominant factor affecting performance. Large errors are not consistently associated with

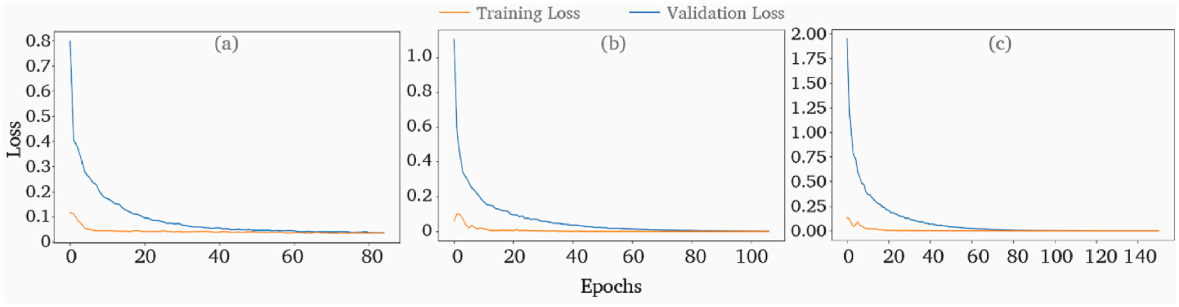

Fig. 5. Training and validation loss for the ANN models requiring the highest number of epochs (a–c).

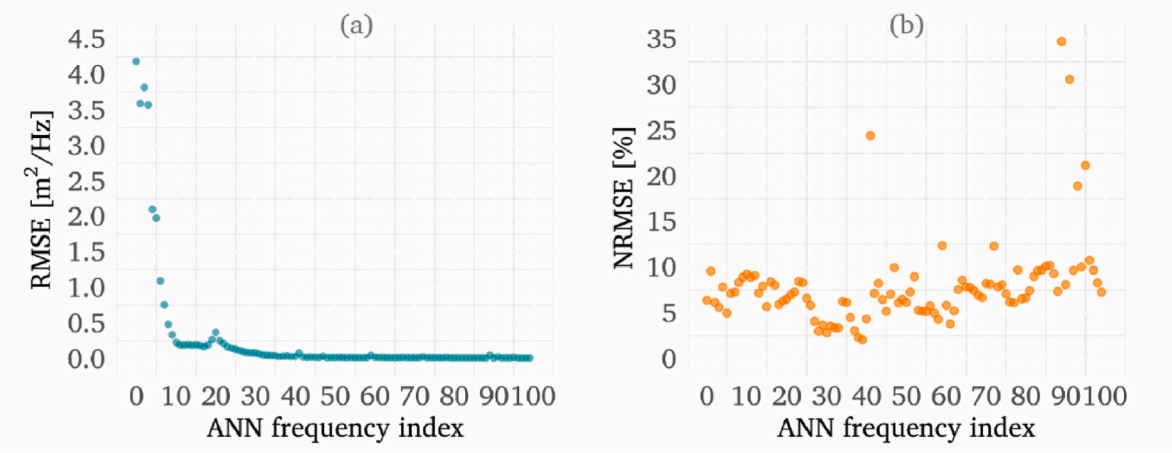

Fig. 6. Distribution of RMSE (a) and NRMSE (b) values for the trained ANNs across different frequency indices.

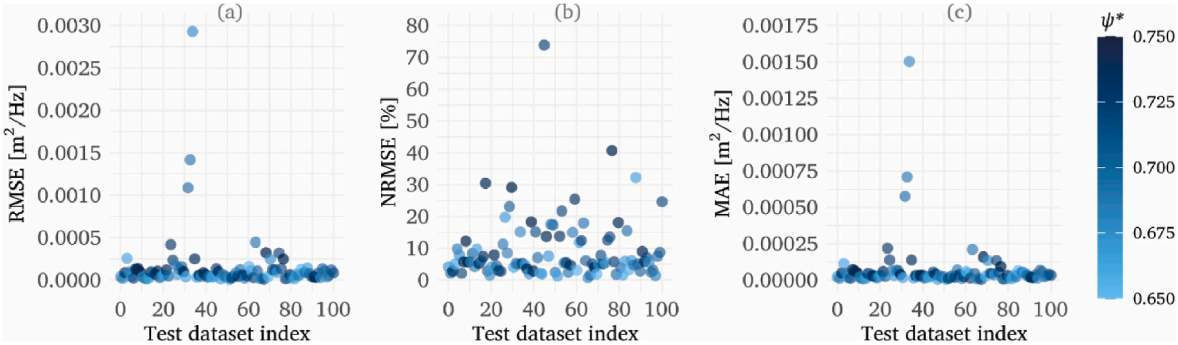

Fig. 7. Error metrics—RMSE (a), NRMSE (b), and MAE (c)—across the 100 records used to evaluate the extrapolation framework, shown in relation to the narrow-bandedness parameter (ψ^*).

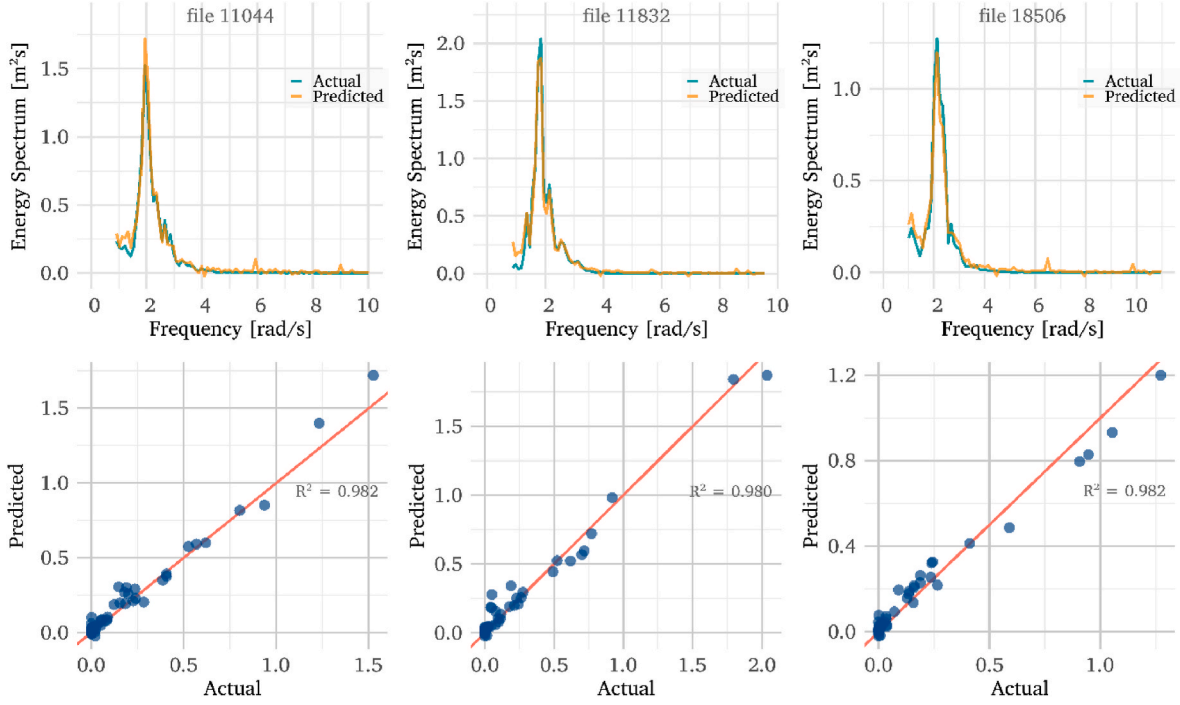

Fig. 8. Comparison of actual and predicted sea surface energy spectrum $S_\eta(\omega)$ (a–c) and the corresponding scatter plots (d–f) for three records used to evaluate the extrapolation framework.

either more irregular sea states (low ψ^*) or narrow-banded conditions (high ψ^*). Overall, most points cluster in low-error regions, highlighting the robustness of the trained ANNs when applied in a full-spectrum extrapolation framework.

Fig. 8 Compares actual and predicted SSE spectra in the frequency domain (a-c) along with corresponding scatter plots (d-f) for three representative records, from the 100 previously unseen cases used to evaluate the extrapolation framework. The predicted spectra closely follow the actual spectra, accurately capturing peak frequencies and energy distributions, with minor discrepancies at higher frequencies where energy content is low. The scatter plots show a strong alignment of data points along the 1:1 line, indicating high predictive accuracy, supported by R^2 values around 0.980. These results demonstrate the model's ability to explain over 98 % of the data variance, with minimal deviations at higher actual values. Given the absence of directly comparable studies in physical experiments, to the best of the authors' knowledge, these findings provide a valuable reference for future research on ANN-based SSE spectrum extrapolation, providing a foundation for further methodological developments.

While the proposed framework demonstrates strong predictive performance under the examined conditions, several limitations should be acknowledged. The NOEL dataset used for model development reflects the prevailing conditions at the measurement site, which are characterized by relatively low, wind-driven sea states and a configuration involving both pressure sensors and ultrasonic probes. As such, the framework has not been validated in environments characterised by strong nonlinearities—such as wave breaking, shallow-water interactions, or storm conditions—where linear theory may no longer be valid. Its generalisation to different sensor configurations or geographic locations may also be constrained if the training data is not sufficiently representative. Nevertheless, the approach can be readily applied to other nearshore environments or field stations that employ similar instrumentation and experience comparable sea states. Finally, although the modular ANN architecture results in increased computational cost, the framework remains computationally feasible and can be executed on a typical personal computer without requiring specialised hardware. This choice was motivated by preliminary tests, in which alternative architectures—such as global ANNs—exhibited unstable training and reduced accuracy. In contrast, the frequency-specific formulation adopted here, guided by the physical interpretation of wave spectra and grounded in the analytical independence of frequency components, proved more effective in this context, resulting in stable training and improved accuracy.

4. Conclusions

This study presents a neural network framework for extrapolating SSE spectrum from pressure measurements in the frequency domain. By decomposing pressure signals into discrete frequency components and training separate ANNs for each frequency, the proposed approach effectively describes the spectral characteristics of the wave field. The extrapolation framework was evaluated on 100 previously unseen records using error metrics such as RMSE, NRMSE, and MAE, with results indicating accurate predictions across most frequencies.

Spectral features were used as input variables to estimate SSE spectrum $S_\eta(\omega)$, offering an alternative approach to traditional time-domain methods, particularly when dealing with missing data and sensor failures. Applying outlier handling in raw data through compressive sampling, transforming it into the frequency domain and normalising proved an effective preprocessing strategy.

The methodology demonstrated generalisation capabilities, with most models converging within 50 epochs. The RMSE was close to zero across most frequencies, with larger values observed at lower frequencies—an expected outcome due to the higher energy content in this range. However, these components contribute relatively little to the overall signal and can be reasonably disregarded. At higher frequencies, variations were less pronounced, reflecting the lower energy associated with those components. When evaluated using the more informative, scale-independent NRMSE metric, most frequency-specific ANNs achieved errors below 13 %, with only a few outliers, thereby demonstrating the robustness and accuracy of the proposed framework.

The narrow-bandedness parameter ψ^* did not show a consistent influence on model performance, suggesting that the framework generalises well across different spectral shapes within the examined range. This is further supported by the strong agreement between actual and predicted spectra observed in Fig. 8, with R^2 values around 0.980 across representative cases. These results indicate that the approach is suitable for the sea states examined in this study, which are representative of wind-generated waves.

In addition to its predictive performance, the proposed framework introduces a modular architecture that reflects the analytical independence of frequency components and enables independent development and evaluation of each ANN. This structure allows for the identification of frequency-specific modelling issues and improves uncertainty control compared to more compact or global ANN architectures.

The proposed framework has practical implications for ocean engineering applications that involve oceanographic monitoring and where reliable wave data reconstruction is required.

Future studies could examine the application of this framework to a wider range of sea states, including swell-dominated environments, consider the inclusion of additional input features, or investigate other machine learning architectures, such as convolutional neural networks (CNNs) or genetic algorithm-assisted CNNs (GA + CNNs), to evaluate potential differences in predictive performance.

CRediT authorship contribution statement

Nikolas Martzikos: Writing – review & editing, Writing – original draft, Visualization, Validation, Software, Resources, Methodology, Investigation, Formal analysis, Data curation, Conceptualization. **Giovanni Malara:** Writing – review & editing, Writing – original draft, Validation, Supervision, Software, Project administration, Methodology, Conceptualization. **Felice Arena:** Writing – review & editing, Writing – original draft, Supervision, Project administration, Methodology, Investigation, Funding acquisition, Conceptualization.

Data availability

Data are not publicly available due to privacy restrictions. Data can be made available upon request to the authors

Declaration of competing interest

The authors declare that they have no known competing financial interests or personal relationships that could have appeared to influence the work reported in this paper.

Acknowledgements

This work was funded by the Next Generation EU - Italian NRRP, Mission 4, Component 2, Investment 1.5, call for the creation and strengthening of 'Innovation Ecosystems', building 'Territorial R&D Leaders' (Directorial Decree n. 2021/3277) - project Tech4You - Technologies for climate change adaptation and quality of life improvement, n. ECS0000009. This work reflects only the authors' views and opinions, neither the Ministry for University and Research nor the European Commission can be considered responsible for them.

References

Benetazzo, A., Fedele, F., Gallego, G., Shih, P.-C., Yezzi, A., 2012. Offshore stereo measurements of gravity waves. Coast. Eng. 64, 127–138. https://doi.org/10.1016/j.coastaleng.2012.01.007.

Boccotti, P., 2000a. Chapter 8 analysis of the sea states in the space-time. In: Wave Mechanics for Ocean Engineering, pp. 249–279. https://doi.org/10.1016/S0422-9894(00)80034-3.

Boccotti, P., 2000b. Chapter 4 wind generated waves: basic concepts. In: Paolo, B. (Ed.), Wave Mechanics for Ocean Engineering, pp. 119–151. https://doi.org/10.1016/S0422-9894(00)80030-6.

Boccotti, P., Arena, F., Fiamma, V., Romolo, A., Barbaro, G., 2011. Estimation of mean spectral directions in random seas. Ocean Eng. 38, 509–518. https://doi.org/10.1016/j.oceaneng.2010.11.018.

Box, G.E.P., Jenkins, G.M., Reinsel, G.C., Ljung, G.M., 2015. Time Series Analysis: Forecasting and Control, fifth ed., fifth ed. Willey.

Campos, R.M., Costa, M.O., Almeida, F., Guedes Soares, C., 2021. Operational wave forecast selection in the Atlantic Ocean using random forests. J. Mar. Sci. Eng. 9, 298. https://doi.org/10.3390/jmse9030298.

Candès, E.J., Romberg, J.K., Tao, T., 2006. Stable signal recovery from incomplete and inaccurate measurements. Commun. Pure Appl. Math. 59, 1207–1223. https://doi.org/10.1002/cpa.20124.

Candes, E.J., Wakin, M.B., 2008. An introduction to compressive sampling. IEEE Signal Process. Mag. 25, 21–30. https://doi.org/10.1109/MSP.2007.914731.

Donoho, D.L., 2006. Compressed sensing. IEEE Trans. Inf. Theor. 52, 1289–1306. https://doi.org/10.1109/TIT.2006.871582.

Durán-Rosal, A.M., Hervás-Martínez, C., Tallón-Ballesteros, A.J., Martínez-Estudillo, A. C., Salcedo-Sanz, S., 2016. Massive missing data reconstruction in ocean buoys with evolutionary product unit neural networks. Ocean Eng. 117, 292–301. https://doi.org/10.1016/j.oceaneng.2016.03.053.

Evensen, G., 2003. The ensemble kalman filter: theoretical formulation and practical implementation. Ocean Dyn. 53, 343–367. https://doi.org/10.1007/s10236-003-0036-9.

Fan, S., Xiao, N., Dong, S., 2020. A novel model to predict significant wave height based on long short-term memory network. Ocean Eng. 205, 107298. https://doi.org/10.1016/j.oceaneng.2020.107298.

Gambarelli, L., Pasta, E., Giorgi, G., 2024. Interpolation techniques: a possible way to bypass offshore resource assessment limitations?. In: Innovations in Renewable Energies Offshore. CRC Press, London, pp. 19–26. https://doi.org/10.1201/9781003558859-3.

Ge, M., Kerrigan, E.C., 2016. Short-term ocean wave forecasting using an autoregressive moving average model. In: 2016 UKACC 11th International Conference on Control (CONTROL). IEEE, pp. 1–6. https://doi.org/10.1109/CONTROL.2016.7737594.

Jörges, C., Berkenbrink, C., Stumpe, B., 2021. Prediction and reconstruction of ocean wave heights based on bathymetric data using LSTM neural networks. Ocean Eng. 232, 109046. https://doi.org/10.1016/j.oceaneng.2021.109046.

Kagemoto, H., 2020. Forecasting a water-surface wave train with artificial intelligence- A case study. Ocean Eng. 207, 107380. https://doi.org/10.1016/j.oceaneng.2020.107380.

Laface, V., Kougioumtzoglou, I.A., Malara, G., Arena, F., 2017. Efficient processing of water wave records via compressive sensing and joint time-frequency analysis via harmonic wavelets. Appl. Ocean Res. 69, 1–9. https://doi.org/10.1016/j.apor.2017.09.011.

Li, C.B., Choung, J., 2017. Fatigue damage analysis for a floating offshore wind turbine mooring line using the artificial neural network approach. Ships Offshore Struct. 12, S288–S295. https://doi.org/10.1080/17445302.2016.1254522.

Li, J., Tong, Y., Xu, Y., Chen, W., Shi, P., 2025. Reconstruction of significant wave height for bottom-mounted acoustic profilers with pressure sensor failure: a case study. Ocean Eng. 319, 120270. https://doi.org/10.1016/j.oceaneng.2024.120270.

Malara, G., 2022. Compressive sampling - based extrapolation of free surface displacement data from pressure measurements. Ocean Eng. 266, 113044. https://doi.org/10.1016/j.oceaneng.2022.113044.

Malara, G., Kougioumtzoglou, I.A., Arena, F., 2018. Extrapolation of random wave field data via compressive sampling. Ocean Eng. 157, 87–95. https://doi.org/10.1016/j.oceaneng.2018.03.044.

Martzikos, N., Ruzzo, C., Malara, G., Fiamma, V., Arena, F., 2024. Applying neural networks to predict offshore platform dynamics. J. Mar. Sci. Eng. 12. https://doi.org/10.3390/jmse12112001.

Martzikos, N., Soukissian, T.H., 2017. Modelling of the sea surface elevation based on a data analysis in the Greek seas. Appl. Ocean Res. 69. https://doi.org/10.1016/j.apor.2017.10.008.

Massel, S.R., 2001. Wavelet analysis for processing of ocean surface wave records. Ocean Eng. 28, 957–987. https://doi.org/10.1016/S0029-8018(00)00044-5.

Minuzzi, F.C., Farina, L., 2024. Artificial neural networks ensemble methodology to predict significant wave height. Ocean Eng. 300, 117479. https://doi.org/10.1016/j.oceaneng.2024.117479.

Ochi, M.K., 1998. Ocean Waves. Cambridge University Press. https://doi.org/10.1017/CBO9780511529559.

Panda, J.P., 2023. Machine learning for naval architecture, ocean and marine engineering. J. Mar. Sci. Technol. 28, 1–26. https://doi.org/10.1007/s00773-022-00914-5.

Pandian, P.K., Emmanuel, O., Ruscoe, J.P., Side, J.C., Harris, R.E., Kerr, S.A., Bullen, C. R., 2010. An overview of recent technologies on wave and current measurement in coastal and marine applications. J. Oceanogr. Mar. Sci. 1, 1–10.

Portillo Juan, N., Matutano, C., Negro Valdecantos, V., 2023. Uncertainties in the application of artificial neural networks in ocean engineering. Ocean Eng. 284, 115193. https://doi.org/10.1016/j.oceaneng.2023.115193.

Portillo Juan, N., Negro Valdecantos, V., 2022. Review of the application of artificial neural networks in ocean engineering. Ocean Eng. 259, 111947. https://doi.org/10.1016/j.oceaneng.2022.111947.

Sidarta, D.E., Lim, H.-J., Kyoung, J., Tcherniguin, N., Lefebvre, T., O'Sullivan, J., 2019. Detection of mooring line failure of a spread-moored FPSO: part 1 — development of an artificial neural network based model. In: Volume 1: Offshore Technology; Offshore Geotechnics. American Society of Mechanical Engineers. https://doi.org/10.1115/OMAE2019-96288.

TensorFlow Developers, 2024. TensorFlow (v2.18.0), Zenodo. https://doi.org/10.5281/zenodo.13989084.

Wei, Z., Davison, A., 2022. A convolutional neural network based model to predict nearshore waves and hydrodynamics. Coast. Eng. 171, 104044. https://doi.org/10.1016/j.coastaleng.2021.104044.

Yuan, L., Chen, Y., Li, Z., 2024. Real-time prediction of mooring tension for semi-submersible platforms. Appl. Ocean Res. 146, 103967. https://doi.org/10.1016/j.apor.2024.103967.

Zanganeh, M., 2017. Simultaneous optimization of clustering and fuzzy IF-THEN rules parameters by the genetic algorithm in fuzzy inference system-based wave predictor models. J. Hydroinform. 19, 385–404. https://doi.org/10.2166/hydro.2017.045.